

# Electrochemistry and Spin-Crossover Behavior of Fluorinated Terpyridine-Based Co(II) and Fe(II) Complexes

Maite Nößler,<sup>[a]</sup> René Jäger,<sup>[a]</sup> David Hunger,<sup>[c]</sup> Marc Reimann,<sup>[d]</sup> Tobias Bens,<sup>[b]</sup> Nicolás I. Neuman,<sup>[b, e]</sup> Arijit Singha Hazari,<sup>[b]</sup> Martin Kaupp,<sup>[d]</sup> Joris van Slageren,<sup>\*,[c]</sup> and Biprajit Sarkar<sup>\*,[a, b]</sup>

Due to their ability to form stable molecular complexes that have tailor-made properties, terpyridine ligands are of great interest in chemistry and material science. In this regard, we prepared two terpyridine ligands with two different fluorinated phenyl rings on the backbone. The corresponding Co<sup>II</sup> and Fe<sup>II</sup> complexes were synthesized and characterized by single-crystal X-ray structural analysis, electrochemistry and temperature-dependent SQUID magnetometry. Single crystal X-ray diffraction analyses at 100 K of these complexes revealed Co–N and Fe–N bond lengths that are typical of low spin Co<sup>II</sup> and Fe<sup>II</sup>

centers. The metal centers are coordinated in an octahedral fashion and the fluorinated phenyl rings on the backbone are twisted out of the plane of the terpyridine unit. The complexes were investigated with cyclic voltammetry and UV/Vis-NIR spectroelectrochemistry. All complexes show a reversible oxidation and several reduction processes. Temperature dependent SQUID magnetometry revealed a gradual thermal SCO behavior in two of the complexes, while EPR spectroscopy provided further insights on the electronic structure of the metal complexes, as well as site of reduction.

## Introduction

An important class of chelating ligands are the 2,2':6',2''-terpyridines (TPYs). These ligands coordinate to different transition-metal ions of various oxidation states and form stable complexes.<sup>[1]</sup> Since the initial synthesis of terpyridine in 1932<sup>[2]</sup> several different synthetic methods have been developed for its synthesis. These include, amongst others, a Pd(0)-catalyzed pyridine coupling,<sup>[3]</sup> Hiyama,<sup>[4]</sup> Stille<sup>[5]</sup> or Suzuki cross-coupling or oxidation of diacetylpyridine and condensation with an

aldehyde.<sup>[6]</sup> But there are still limitations regarding the efficient synthesis of structurally diverse terpyridine ligands and those bearing electronically different substituents.<sup>[7]</sup> There is a wide range of applications of metal complexes containing one or two terpyridine ligands: electrocatalysis for proton<sup>[8]</sup> or CO<sub>2</sub> reduction<sup>[8a,9]</sup> and water oxidation,<sup>[10]</sup> photosensitizers,<sup>[11]</sup> redox shuttles for dye sensitized solar cells (DSSC),<sup>[12]</sup> supramolecular polymers,<sup>[13]</sup> nonlinear optics,<sup>[14]</sup> ion sensors<sup>[15]</sup> or anolytes for redox flow batteries<sup>[16]</sup> to name only a few examples. Furthermore, a high potential in clinical applications for complexes bearing a tpy unit has been reported.<sup>[17]</sup> The complexes are able to intercalate with DNA and for example the cytotoxicity of Ru(TPY)Cl<sub>2</sub> was investigated, which exhibits activity against certain leukemia cells in between the activity of cisplatin and carboplatin.<sup>[17b]</sup>

Terpyridine complexes can behave as spin-crossover systems and are hence of great interest for their potential use as sensors,<sup>[18]</sup> switches and memory devices.<sup>[19]</sup> Spin-crossover (SCO), known as the reversible switching between a low-spin (LS) and a high-spin (HS) state of a molecule, occurs typically in octahedrally coordinated transition-metal complexes with a d<sup>4</sup>–d<sup>7</sup> electronic configuration. The SCO can be stimulated by external stimuli such as pressure, light, temperature or electric fields.<sup>[19b,c]</sup> Most commonly Co<sup>II</sup> and Fe<sup>II</sup> complexes have been studied, with Fe<sup>III</sup>-based SCO complexes being an overwhelming majority.<sup>[20]</sup>

Over recent years, materials that exhibit synergistic coexistence of two or more properties (multifunctional molecular materials) have received attention due to their potential applications in sensors, electrooptic devices, information storage and spintronics.<sup>[21]</sup> In such applications, the more attractive multifunctional molecule-based materials are SCO compounds, which are coupled for example with electrical conductivity,<sup>[22]</sup> liquid crystalline behavior,<sup>[23]</sup> non-linear optical (NLO)<sup>[24]</sup> and/or

[a] M. Nößler, R. Jäger, Prof. Dr. B. Sarkar  
Institut für Chemie und Biochemie  
Freie Universität Berlin  
Fabeckstraße 34–36, D-14195, Berlin (Germany)

[b] T. Bens, Dr. N. I. Neuman, Dr. A. Singha Hazari, Prof. Dr. B. Sarkar  
Institut für Anorganische Chemie  
Universität Stuttgart  
Pfaffenwaldring 55, D-70569 Stuttgart (Germany)  
E-mail: biprajit.sarkar@iac.uni-stuttgart.de  
http://www.iac.uni-stuttgart.de/en/research/aksarkar/

[c] D. Hunger, Prof. Dr. J. van Slageren  
Institut für Physikalische Chemie  
Universität Stuttgart  
Pfaffenwaldring 55, 70569 Stuttgart (Germany)  
E-mail: slageren@ipc.uni-stuttgart.de  
http://www.ipc.uni-stuttgart.de/slageren/

[d] Dr. M. Reimann, Prof. Dr. M. Kaupp  
Technische Universität Berlin  
Institut für Chemie, Theoretische Chemie/Quantenchemie  
Sekr C7, Straße des 17. Juni 135, D-10623 Berlin (Germany)

[e] Dr. N. I. Neuman  
Instituto de Desarrollo Tecnológico para la Industria Química  
INTEC, UNL-CONICET Paraje El Pozo, Santa Fe (Argentina)

Supporting information for this article is available on the WWW under <https://doi.org/10.1002/ejic.202300091>

© 2023 The Authors. European Journal of Inorganic Chemistry published by Wiley-VCH GmbH. This is an open access article under the terms of the Creative Commons Attribution License, which permits use, distribution and reproduction in any medium, provided the original work is properly cited.

luminescence properties.<sup>[25]</sup> More recently, the group of Hayami investigated a Co<sup>II</sup> complex bearing a terpyridine unit with a ((3-fluorophenyl)ethynyl) substituent in the para position of the central pyridine ring (FPh-terpy), that exhibit SCO behavior that is dependent on the degree of motion of the fluorophenyl ring. A ferroelectric hysteresis loop and spontaneous polarization is induced due to an electrically reversible dipole moment which results from the motion.<sup>[26]</sup>

The SCO properties of a bulk sample can be dramatically influenced by tuning the interactions between the SCO molecules the sample is based on.<sup>[27]</sup> In order to design new materials that might be applicable in information technology, it is important to understand the cooperative behavior in SCO transition.<sup>[27]</sup> One possible way to influence this behavior is to increase the flexibility of the ligands by attaching long alkyl groups.<sup>[27–28]</sup> In this regard the group of Hayami extensively studied Co<sup>II</sup> complexes containing terpyridine ligands with long alkyl chains with respect to their SCO behavior.<sup>[27,29]</sup> Moreover, these complexes also exhibit liquid crystalline properties.

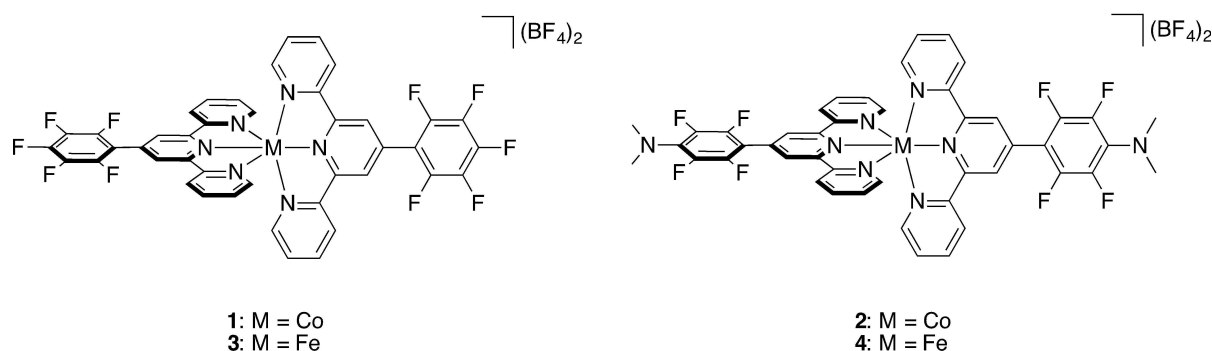
The investigation presented in this work includes the synthesis of two Co<sup>II</sup> and two Fe<sup>II</sup> complexes with terpyridine ligands containing fluorinated substituents (Scheme 1). These substituents were introduced to either tune the properties of the metal complexes (fluorine as the most electronegative element, possible F-specific interactions), or to introduce additional functionalities (e.g. the redox-active dimethyl-amino group). Both of the aforementioned substituents are expected to affect the electrochemical and the spectroscopic properties

of the metal complexes. Additionally, the fluorinated substituents can potentially engage in fluorine-specific interactions which can influence the magnetic properties of the resulting metal complexes. The complexes were characterized through crystallographic methods, cyclic voltammetry as well as UV/Vis/NIR spectroelectrochemistry and EPR spectroscopy. Additionally, the SCO behavior was investigated through temperature dependent SQUID magnetometry.

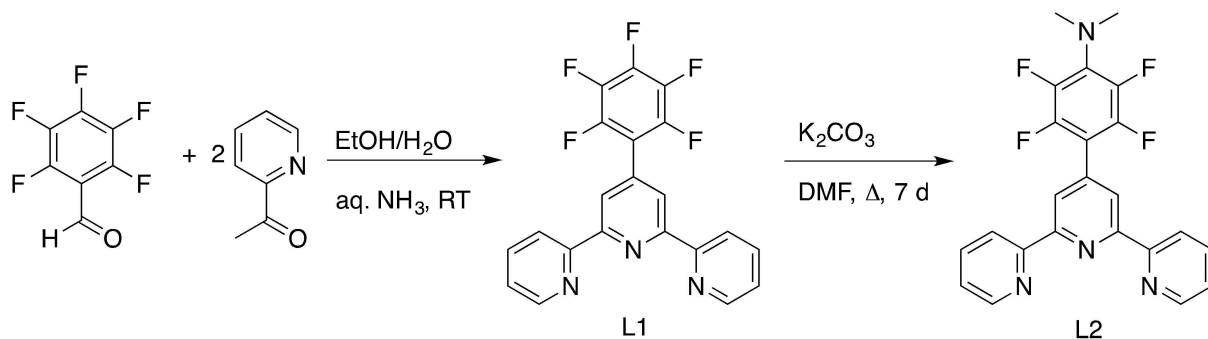
## Results and Discussion

### Synthesis and Structural Characterization

2,3,4,5,6-pentafluorobenzaldehyde was reacted with 2-acetylpyridine to yield ligand 1 according to a published procedure (Scheme 2).<sup>[30]</sup> Ligand 2 was synthesized by stirring 4'-(perfluorophenyl)-2,2':6',2''-terpyridine in *N,N*-dimethylformamide. The corresponding homoleptic complexes containing two of these ligands were synthesized by reacting the metal salt (Co(BF<sub>4</sub>)<sub>2</sub>·6 H<sub>2</sub>O or Fe(BF<sub>4</sub>)<sub>2</sub>·6 H<sub>2</sub>O) with the ligands in a stoichiometric ratio of 1:2 in methanol at room temperature (See Experimental Section). All complexes were easily purified by dissolution of the complex in acetonitrile and suspension in diethylether. The resulting precipitates were filtered and the newly synthesized complexes were characterized by mass spectrometry, elemental analysis and, in case of complexes 1–3, by X-ray diffraction. The cobalt complexes are paramagnetic,



Scheme 1. New Co<sup>II</sup> and Fe<sup>II</sup> terpyridine complexes presented in this work.



Scheme 2. Synthesis of ligands 1 and 2.

which was confirmed with  $^1\text{H}$  NMR spectra showing peaks up to 55 ppm, whereas the iron complexes are diamagnetic at room temperature, yielding diamagnetic  $^1\text{H}$  NMR spectra in *d*<sup>3</sup>-acetonitrile (See Supporting Information). This observation of low-spin  $\text{Fe}^{\text{II}}$  centers under ambient conditions was also reported with other  $\text{Fe}^{\text{II}}$  terpyridine-based complexes.<sup>[31]</sup>

It was possible to obtain suitable single crystals of three of the complexes by slow diffusion of diethylether in acetonitrile solutions. All the complexes crystallize in the orthorhombic *Fdd2* space group and show the expected coordination motif. The metal center is coordinated in an octahedral fashion through the three nitrogen atoms of each ligand (Figure 1). The  $\text{Co-N6}$  octahedron is highly distorted as can be seen from the shorter  $\text{Co-N}$  distance to the central pyridyl-N atoms compared to the peripheral pyridyl-N atoms (Table 1). The fluorinated phenyl rings on the backbone are twisted out of the plane of the terpyridine unit. The bond lengths between 1.880 (7) and 2.152 (4) Å indicate a LS center for the  $\text{Co}^{\text{II}}$  complexes **1** and **2**<sup>[19c]</sup> and the bond lengths between 1.862 (7) and 1.980 (4) Å also point towards a LS center for the  $\text{Fe}^{\text{II}}$  complex **3** at the measured temperature of 100 K.<sup>[32]</sup>

The bond angles in and between the terpyridine rings and the metal center are similar for **1** and **3**. The angles of **2** show a larger distortion in the bond angles for one terpyridine unit with a difference up to 6° in comparison to **1** (for the  $\text{N3-M-N3}$  angle). Selected bond angles of the complexes are depicted in Table 2. The longer bond distances of  $\text{Co-N3}$  of 0.2 Å support this observation. It appears that the introduction of the  $\text{NMe}_2$  groups has an influence on the  $\text{N-M-N}$  angles, since the values

differ from those of the complexes with the pentafluorophenyl ring. The angle between the planes of the tridentate ligands are nearly perpendicular to one another with values of 89.1° for complex **1**, 87.9° for complex **2** and 88.9° for complex **3**. The contact bond of 7.123 (2) Å between two nearest-neighbors of complex **1** is rather long, and similar values are also observed for the other two complexes. No specific fluorine specific interactions were observed. Nevertheless, the packing of the molecules is as expected (figure 2). The terpyridine units are face to face to one another and the  $\text{BF}_4^-$  anions and solvent molecules are arranged between the sheets (see Supporting Information).

### Cyclic Voltammetry

In order to investigate the influence of the metal center and the substituents on the terpyridine ligands on the redox properties of the complexes, cyclic voltammograms were recorded in anhydrous dichloromethane and acetonitrile solutions. The redox potentials for selected processes are given in Table 3.

Cyclic voltammetry reveals that all complexes show at least one reversible oxidation for the  $\text{M}^{\text{II}}/\text{M}^{\text{III}}$  redox couple (in a 0.1 M  $\text{NBu}_4\text{PF}_6$  dichloromethane solution).<sup>[33]</sup> In case of **2** and **3** a second irreversible oxidation is observed (see Supporting Information).

Both the cobalt complexes display a large peak-to-peak separation for the oxidation waves with  $\Delta E_p$  of 164 mV for **1** and 104 mV for **2** for the first oxidation, whereas values of

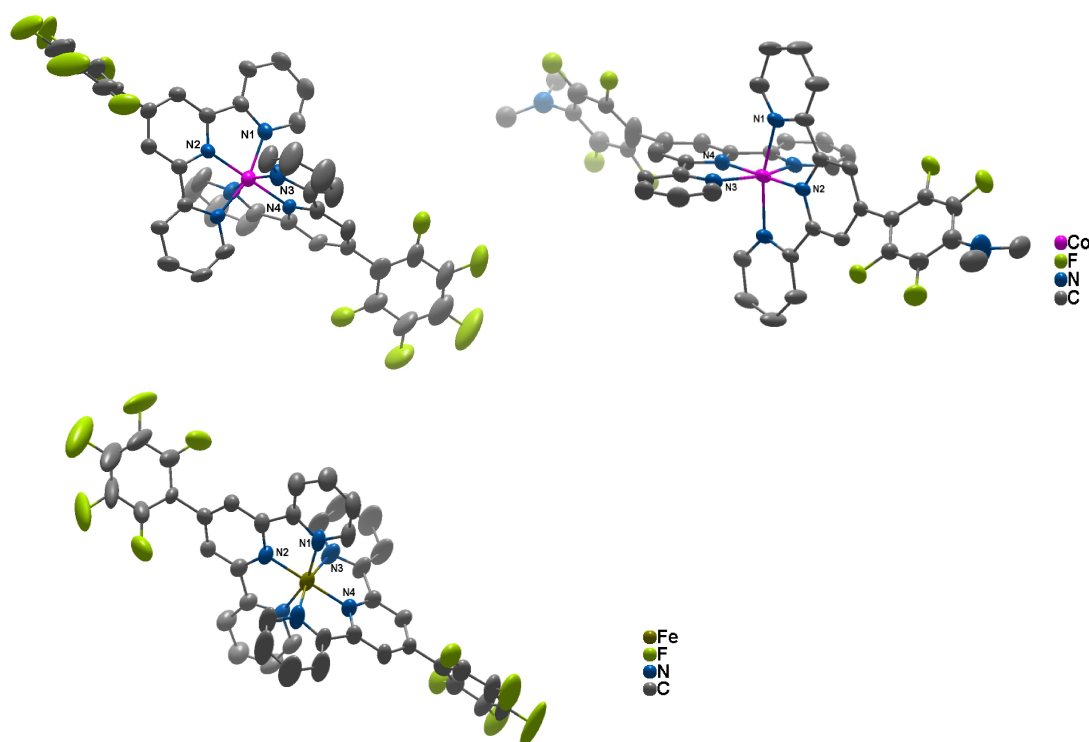
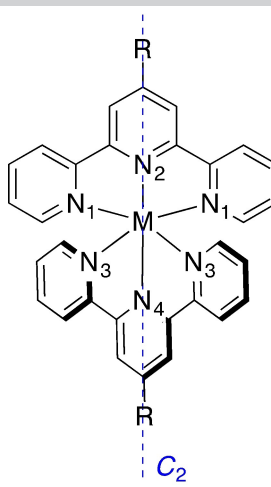


**Figure 1.** Perspective view of cobalt complexes **1** and **2** and iron complex **3** (disordered atoms were deleted, for a complete representation see Figure S12). Ellipsoids are at a probability level of 50%. H atoms, anions and solvent molecules are omitted for clarity.

**Table 1.** Selected bond lengths of complexes 1–3.



	M–N1	M–N2	M–N3	M–N4
<b>1</b>	1.968 (4)	1.880 (7)	1.976 (4)	1.894 (6)
<b>2</b>	2.022 (3)	1.891 (5)	2.152 (4)	1.949 (5)
<b>3</b>	1.966 (6)	1.86 (1)	1.979 (6)	1.90 (1)
Co[TPYOC <sub>14</sub> H <sub>29</sub> ] <sub>2</sub> (BF <sub>4</sub> ) <sub>2</sub> [a] <sup>[29]</sup>	2.137(4)/2.114(4)	1.910(3)	1.977(4)/ 1.976(4)	1.844(3)
Fe[N <sub>3</sub> P <sub>3</sub> (OPh) <sub>5</sub> (OPhTPY)] <sub>2</sub> (PF <sub>6</sub> ) <sub>2</sub> [b] <sup>[32]</sup>	1.886 (3)	1.987 (3)	1.995 (3)	1.976 (3)

[a] Complex with a LS Coll center: [b]Complex with a LS Fell center.

**Table 2.** Selected bond angles of complexes 1–3.

	1	2	3
<b>N1–M–N1</b>	160.9 (3)	160.8 (2)	161.3 (3)
<b>N1–M–N2</b>	80.4 (2)	80.4 (1)	80.6 (2)
<b>N1–M–N3</b>	90.9 (2), 92.0 (2)	91.0 (2), 92.8 (2)	90.3 (2), 92.5 (2)
<b>N1–M–N4</b>	99.5 (2)	99.5 (2)	99.3 (2)
<b>N2–M–N3</b>	98.7 (2)	101.63 (9)	98.8 (2)
<b>N2–M–N4</b>	180.0	180.0	180.0
<b>N3–M–N3</b>	162.4 (3)	156.7 (2)	162.3 (3)
<b>N3–M–N4</b>	81.2 (2)	78.37 (9)	81.1 (2)

88 mV and 83 mV were obtained for the iron complexes **3** and **4** (in CH<sub>2</sub>Cl<sub>2</sub> at a scan rate of 0.1 V). This has been observed earlier for similar systems<sup>[34]</sup> and is probably related to the slow kinetics for electron transfer for such cobalt complexes which have to undergo a large structural reorganization because of their change from a HS Co(II) (predominant form at ambient temperatures) to a LS Co(III) form. The oxidation potentials of the iron complexes **3** and **4** are shifted to more positive potentials compared to their cobalt analogues. This fact is likely related to the removal of an electron from a e<sub>g</sub> orbital in a HS

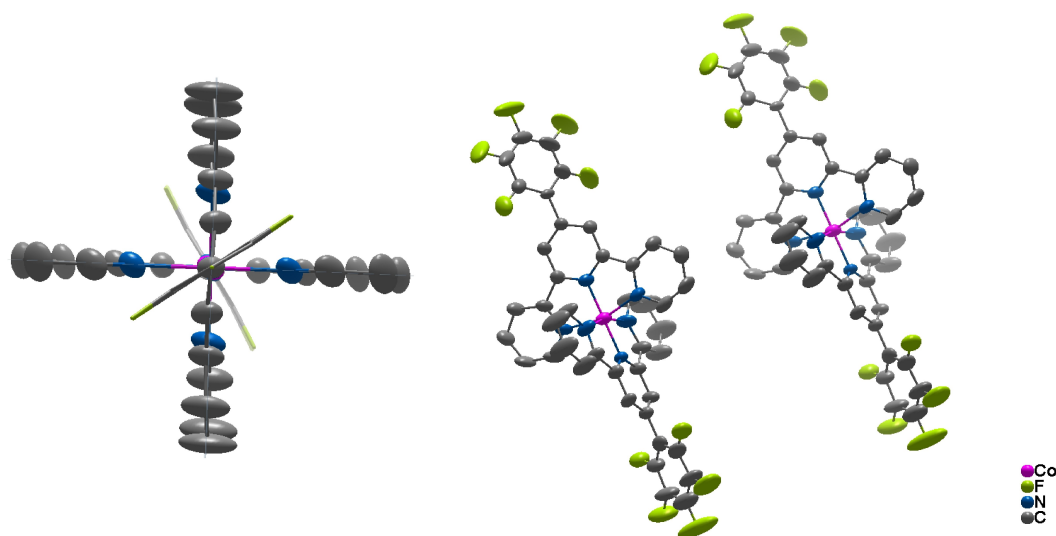


**Figure 2.** Ellipsoid views depicting orthogonality of the ligand planes (left) and neighboring units of complex **1** (right).

Table 3. Redox potentials vs. FcH/FcH <sup>+</sup> measured in CH <sub>2</sub> Cl <sub>2</sub> at 100 mVs <sup>-1</sup> with 0.1 M Bu <sub>4</sub> NPF <sub>6</sub> at room temperature. <sup>[a]</sup>			
	E <sup>Ox</sup> <sub>1/2</sub>	E <sup>Red1</sup> <sub>1/2</sub>	E <sup>Red2</sup> <sub>1/2</sub>
1	-0.06	-0.99	-1.99 <sup>[b]</sup>
2	-0.05	-1.10 <sup>[b]</sup>	-2.24 <sup>[b]</sup>
3	0.85	-1.45	-1.66
4	0.84	-1.46	-1.68

[a] All measured with a glassy carbon electrode. [b] Peak potential for irreversible processes.

Co(II) case in comparison to the removal of an electron from a t<sub>2g</sub> orbital in a LS Fe(II) case. Our calculations at the B97-D/def2-TZVP level clearly support the low-spin nature of both d<sup>6</sup> compounds. For the Co(II) compound, however, both relative energies and the form of the calculated spectrum rather suggest the presence of a low-spin (doublet) ground state (see Section S6 of the Supporting Information). This is consistent with the structures obtained experimentally at 100 K. The effect of the substituents on the ligand on the oxidation potentials of the metal complexes is negligible.

All complexes display two reduction steps. For the cobalt complex 1 the first reduction is reversible, whereas for complex 2 both the first and the second reduction steps are irreversible (Figure 3). At this point it is not completely clear as to why the reversibility of the first reduction step is different for the complexes 1 and 2. A possible reason could be the presence of the additional basic dimethylamino groups on the backbone of the substituted terpyridine ligands in complex 2. Such basic groups might become more susceptible to follow-up reactions on reduction of the complex. In contrast, the iron complexes 3 and 4 both display two reversible reduction steps. Furthermore, the first reduction step for the iron complexes is negatively shifted by about 400 mV compared to those of the cobalt

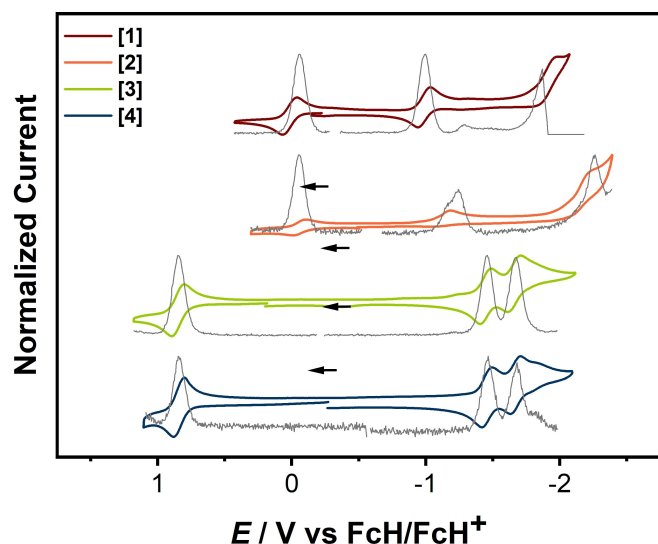


Figure 3. Cyclic voltammograms and differential pulse voltammograms of complexes 1–4 in CH<sub>2</sub>Cl<sub>2</sub>/NBu<sub>4</sub>PF<sub>6</sub> measured with a glassy carbon working electrode (FcH = ferrocene; FcH<sup>+</sup> = ferrocenium).

complexes (Figure 3 and Table 3). We attribute these differences to a predominantly ligand centered reduction step for the iron complexes, and to a more complex electronic situation for the reduced forms of the cobalt complexes (see below). This phenomenon has been observed earlier in different metal complexes with terpyridine ligands,<sup>[35]</sup> but also for for example bis(pyridine-2,6-diimine) cobalt, zinc and iron complexes,<sup>[36]</sup> where it had been assigned to a metal-centered reduction of Co<sup>II</sup> to Co<sup>I</sup>.

The potentials of the redox processes observed in both dichloromethane and acetonitrile solvents only differ slightly (see Table 3). However, in an acetonitrile solution additional redox processes can be observed for complexes 2–4. The additional reduction processes are all irreversible (see Supporting Information). This might be due to disconnection of the ligand and addition of an acetonitrile molecule.<sup>[37]</sup>

### UV/Vis/NIR spectroelectrochemistry

The interplay of the electrochemical and optical properties was probed with UV/Vis/NIR spectroelectrochemistry using an optically transparent thin layer electrochemical (OTTLE) cell. Here, we concentrated on the first oxidation of all the complexes, the first reduction for 1 and 2 and the first two reductions for 3 and 4. Due to strong adsorption of complex 4 on the gold working electrode, which inhibited any optical observations, the complex was measured with a platinum working electrode. In the UV/Vis spectra (shown in figure S8) it is evident that the variations of the ligand backbone do not have a strong effect on the absorption spectrum. Since the complexes with both ligands showed a similar behavior, TD-DFT calculations at the B97-D/def2-TZVP level were performed only for complexes 1 and 3 (for Details, see Section S6 of the Supporting Information). The measured UV/Vis spectra are in good agreement with the calculated ones (see figures S17 and S18 in the Supporting Information).

Figure 4 shows the results of UV/Vis/NIR spectroelectrochemistry for complexes 1 (in CH<sub>2</sub>Cl<sub>2</sub>) and 2 (in CH<sub>3</sub>CN). Upon oxidation of complex 1 (Figure 4a) and 2 (Figure S10e) a decrease in the extinction coefficient was observed (in CH<sub>2</sub>Cl<sub>2</sub>).

Upon reduction of 1 and 2 the band at 500 nm increases in intensity and a new band at around 1300 nm arises (Figure 4b and d). This feature is very different from what is observed for the reduced forms of the iron complexes (see below). DFT (B97-d/def2-TZVP) calculations suggest a distribution of the spin density over both the ligands and the metal, pointing to a complex electronic situation (see Supporting Information, section S6 for details). In line with previous studies on terpyridine-based cobalt complexes of the group of Wieghardt, the bands at 500 nm and 1300 nm might be assigned to metal-to-ligand 3d<sup>8</sup> → 3d<sup>7</sup> π\*1 charge-transfer transitions.<sup>[38]</sup> Since the second reduction of 1 and 2 were irreversible during CV they were not investigated any further. As the native spectra and the end spectrum after reduction of 1 is similar to the native spectrum the process seems to be reversible, while for 2 is

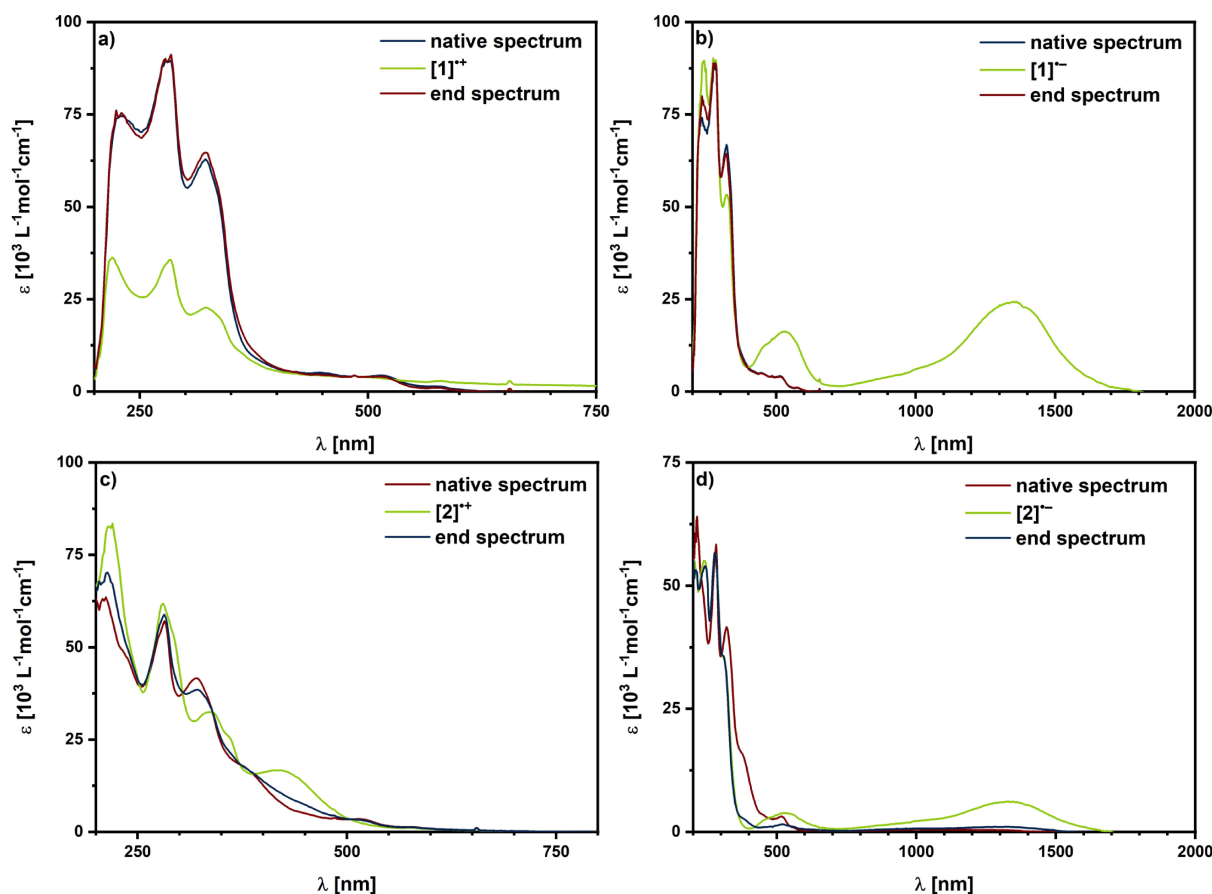


**Figure 4.** UV/Vis SEC spectra of complex 1 top, left: oxidation, right: reduction in  $\text{CH}_2\text{Cl}_2/\text{NBu}_4\text{PF}_6$  measured with a gold working electrode; bottom UV/Vis/NIR spectrum of complex 2 during the oxidation in  $\text{CH}_3\text{CN}/\text{NBu}_4\text{PF}_6$  measured with a gold working electrode.

irreversible, which is in accordance with the data obtained from cyclic voltammetric measurements.

As the spectra for both iron complexes are similar, only the spectra of **3** will be discussed in detail (figure 5a-c). In the native form, **3** and **4** exhibit  $\pi - \pi^*$  transitions below 350 nm and a MLCT band at 560 nm. Additionally, shoulders are observed at around 630 nm which are consistent with iron-centered d-d transitions in related systems.<sup>[32]</sup> Upon oxidation, the band at 560 nm decreases and increases again after re-reduction (figure 5a), showing a reversible oxidation for **3**, which corresponds to an  $\text{Fe}^{\text{II}}$  to  $\text{Fe}^{\text{III}}$  oxidation, as confirmed by calculated natural population analysis (NPA) charges obtained at the DFT level (see Supporting Information, section S6). During the reduction, the MLCT band at 560 nm shifts to higher wavelengths and the appearance of additional shoulders can be observed (figure 5b), which is clearly reproduced by theory (Figure S17 of the Supporting Information).

Overall, the oxidation and first reduction process of **3** are fully reversible, as the native and the end spectrum after the second reduction show a loss in the extinction coefficient (figure 5c). This might be due to structural changes upon reduction or decomposition of the complexes. The reduction overall takes place at the ligand, as is supported by NPA charges (see section S6 of the Supporting Information).

## EPR Spectroscopy

Both  $\text{Co}^{\text{II}}$  complexes **1** and **2** display anisotropic EPR signals in solution and in the solid state at 93 K, with partially resolved hyperfine splittings arising from interaction of the electron spin with the  $^{59}\text{Co}$  nucleus ( $I = 7/2$ ). The EPR spectra obtained from powdered samples of **1** and **2** were simulated with rhombic **g**- and **A**-matrices (values given in Table 4). The *g*-values in the 2.00–2.20 range are consistent with a low-spin  $\text{Co}^{\text{II}}$  center<sup>[39]</sup> and

**Table 4.** Simulation parameters of **1** and **2**. *g*-values, hyperfine *A*-values (MHz), anisotropic Gaussian broadening HS (MHz) and isotropic Gaussian and Lorentzian broadenings (mT).

	1 Powder	$\text{CH}_3\text{CN}$	2 Powder	$\text{CH}_3\text{CN}$
$g_x$	2.022	2.004	2.009	2.033
$g_y$	2.147	2.159	2.178	2.144
$g_z$	2.191	2.199	2.192	2.199
$A_x$ / MHz	52.3	42.3	42.0	75.9
$A_y$ / MHz	84.6	82.9	91.7	173.4
$A_z$ / MHz	271.6	281.7	279.4	287.2
$\text{HS}_x$ / MHz	276.7	4.2	0.2	152.0
$\text{HS}_y$ / MHz	219.8	60.8	123.7	208.7
$\text{HS}_z$ / MHz	89.5	146.2	171.9	81.1
$\text{lwpp}$ / mT	[2.79 3.88]	3.61	[0 2.05]	[0.81 1.04]

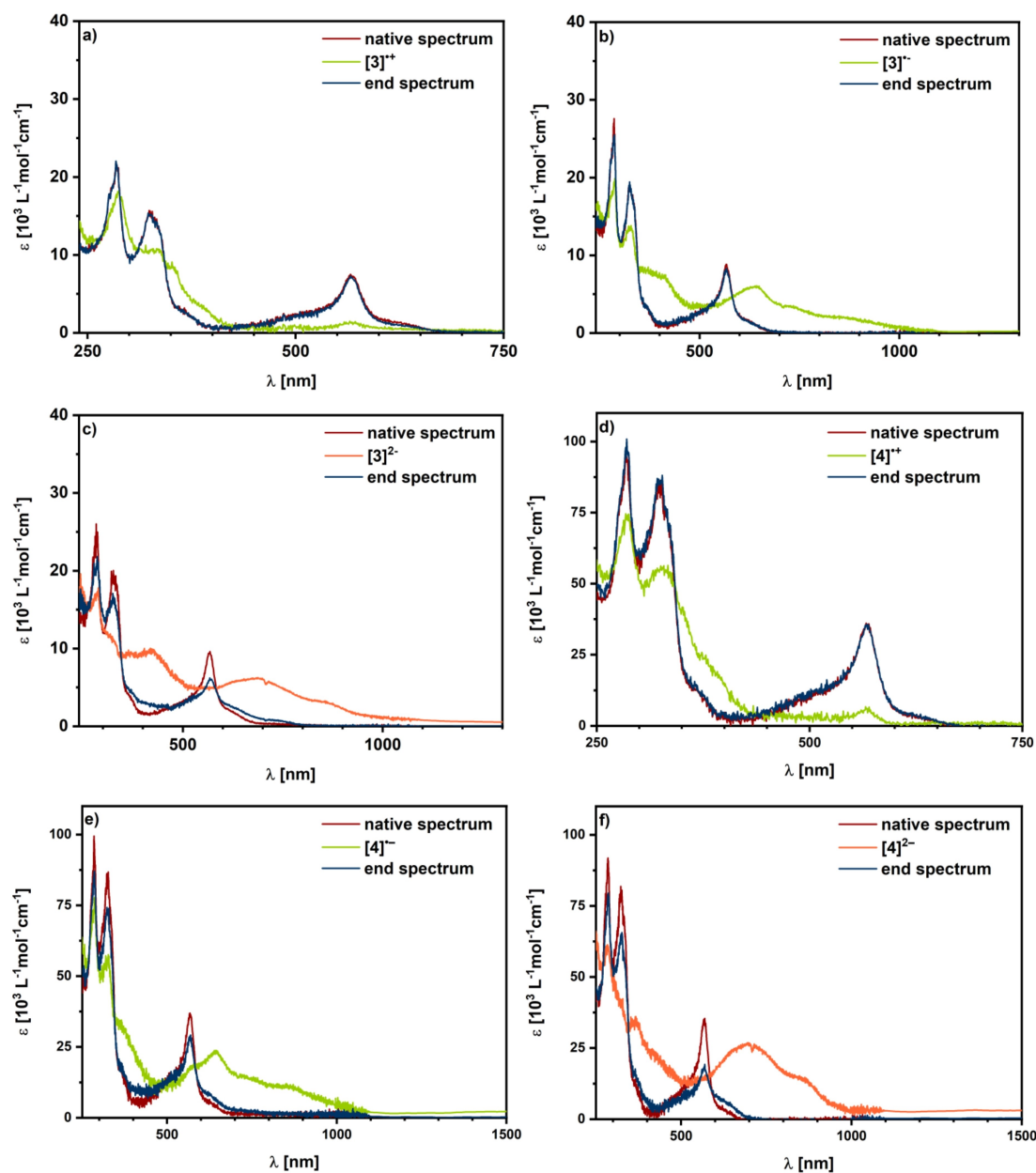


**Figure 5.** UV/Vis SEC spectra of complex 3 (a) oxidation, b) first reduction c) second reduction) in  $\text{CH}_2\text{Cl}_2/\text{NBu}_4\text{PF}_6$  measured with a gold working electrode; UV/Vis SEC spectra of complex 4 (d) oxidation, e) first reduction f) second reduction) in  $\text{CH}_2\text{Cl}_2/\text{NBu}_4\text{PF}_6$  measured with a platinum working electrode.

in agreement with the Co–N distances determined from X-ray diffraction. The rhombic  $g$ -matrices, deviating from the free-electron value of 2, as well as the large hyperfine splittings, clearly indicate a metal centered spin. In a perfectly octahedral environment, the unpaired electron would reside in the degenerate  $e_g$  orbitals. Jahn–Teller distortions lift this degeneracy, which can result in the unpaired electron being either on a  $d_{x^2-y^2}$  or  $d_{z^2}$  orbital, or a mixture of the two, with the  $z$ -axis being that of the axial Jahn–Teller distortion.<sup>[39–40]</sup> The rhombic nature of the  $g$ -values in complexes 1 and 2 indicate that the magnetic orbital is an admixture of the  $d_{x^2-y^2}$  or  $d_{z^2}$  orbitals.

The spectra recorded in the solid state and in solution have similar  $g$ - and  $A$ -values for 1 but show different  $A$ -values for 2.

Additionally, the hyperfine coupling in solution for 2 shows a better resolution (figure 6). These differences are consistent with small changes in the solution and solid-state structures, likely arising from packing effects in the latter.

In addition to the native state of complexes 1 and 2, the one-electron reduced form of complexes 3 and 4 were investigated with EPR spectroelectrochemical measurements. For both complexes a signal, without hyperfine coupling, could be observed after electrolysis at temperatures below 0 °C (Figure 7). The  $g$ -values of 1.983 for both complexes are close to the  $g$ -values of the free electron (Table 5),<sup>[41]</sup> which indicates a ligand-centered spin. These measurements support the assignment of the first reduction being located on the terpyridine

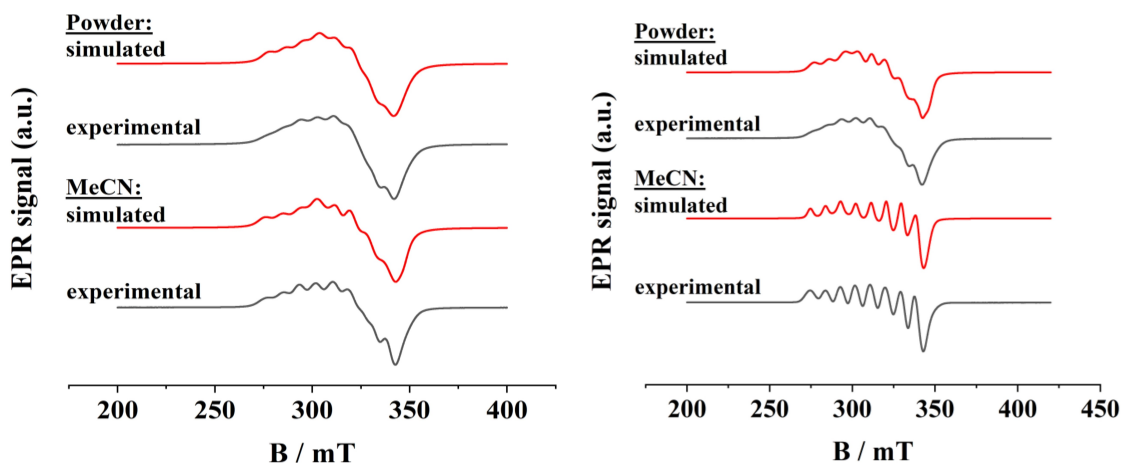


**Figure 6.** Experimental (grey) and simulated (red) EPR spectra of: left:  $\text{Co}(\text{TPYF}_5\text{Ph})_2(\text{BF}_4)_2$  **1** of powdered sample at  $-180^\circ\text{C}$  and in  $\text{CH}_3\text{CN}$  at  $-179^\circ\text{C}$ , right:  $\text{Co}(\text{TPYPhF}_4\text{NMe}_2)_2(\text{BF}_4)_2$  **2** of powdered sample at  $-179^\circ\text{C}$  and in  $\text{CH}_3\text{CN}$  at  $-180^\circ\text{C}$ .

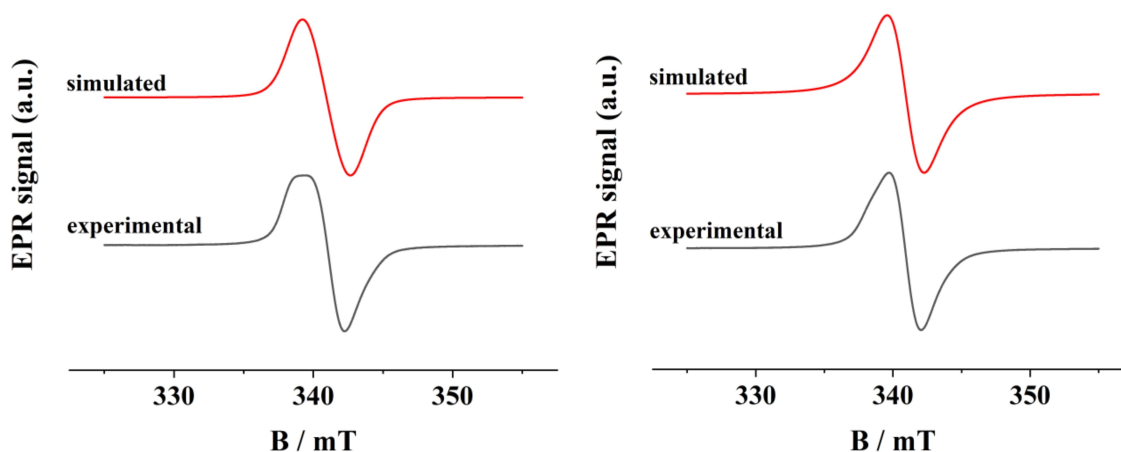


**Figure 7.** Experimental (grey) and simulated (red) EPR spectra of  $\text{Fe}(\text{TPYPhF}_5)_2(\text{BF}_4)_2$  **3** (left) and  $\text{Fe}(\text{TPYPhF}_4\text{NMe}_2)_2(\text{BF}_4)_2$  **4** right during EPR SEC measurements of the first reduction in a  $\text{CH}_2\text{Cl}_2/\text{NBu}_4\text{PF}_6$  measured with a platinum working electrode.

**Table 5.** Simulation parameters for one-electron reduced states of **3** and **4** in a frozen solution of  $\text{CH}_2\text{Cl}_2$ .

Parameters	<b>3</b> Frozen solution	<b>4</b> Frozen solution
g	1.983	1.983
$A_{\text{H}}/\text{MHz}$	10.0	9.0
Line width for isotropic broadening / mT	[2.00]	[1.45]

ligand. The Fe nucleus has no nuclear spin, but the  $^{14}\text{N}$  nuclei in the terpyridine ligands have  $I=1$ . Using the same intrinsic line width ( $\sim 2$  mT) as for the Co complexes resulted in a much too narrow simulated resonance, which did not adequately reproduce the experimental spectra. For this reason, we included in the simulation the (unresolved) hyperfine interaction to three  $^{14}\text{N}$  nuclei, which improved the simulations. The spectra are depicted in figure 7.

## Magnetic Measurements

As the complexes contain  $M^{\text{II}}$  ions in a  $d^6$  or  $d^7$  electronic configuration the metal centers can occur in two spin states (high spin and low spin) and might be reversibly switched between these states by an external stimulus. In this regard, an excellent method for probing the temperature dependent SCO behavior of  $\text{Fe}^{\text{II}}$  and  $\text{Co}^{\text{II}}$  compounds is SQUID magnetometry. If the energy difference from the LS state ( $S=0$  or  $S=1/2$ ) to the HS state ( $S=2$  or  $S=3/2$ ) is provided by thermal energy, a change in the magnetic behavior can be observed.<sup>[42]</sup> For this, complexes **1–3** were investigated by the means of SQUID magnetometry in the temperature  $[T]$  range of 1.8 to 300 K. The  $T$  dependence of the  $\chi T$  product is depicted, where  $\chi$  is the molar static magnetic susceptibility, which can be approximated at low fields as the ration between the molar magnetization and the applied magnetic field.



For the cobalt complexes a gradual thermal SCO behavior is observed from 150 K on with increasing temperature. Due to no strong intermolecular interactions between the SCO units this gradual SCO is expected. The  $\chi_{\text{M}}T$  value for complex 1 increases from  $0.39 \text{ cm}^3\text{Kmol}^{-1}$  at 1.8 K to  $0.42 \text{ cm}^3\text{Kmol}^{-1}$  at 7 K and remains almost constant at  $0.44 \text{ cm}^3\text{Kmol}^{-1}$  up to 150 K. From 150 K the start of the SCO is observed with a gradual increase of the  $\chi_{\text{M}}T$  value from  $0.44 \text{ cm}^3\text{Kmol}^{-1}$  at 150 K to  $0.63 \text{ cm}^3\text{Kmol}^{-1}$  at 300 K.

Complex 2 displays a similar SCO behavior as complex 1. In this case the  $\chi_{\text{M}}T$  value remains almost constant at  $0.59 \text{ cm}^3\text{Kmol}^{-1}$  until it starts increasing upon heating at 150 K. The curve is gradually increasing up to 300 K with a  $\chi_{\text{M}}T$  value of  $0.92 \text{ cm}^3\text{Kmol}^{-1}$ .

Spin-Hamiltonian simulations of the temperature dependence of  $\chi_{\text{M}}T$  based on the parameters obtained by powder EPR of the low spin species of 1 and 2 are shown in figure 8. While for 1, the measured  $\chi_{\text{M}}T$  values between 5 and 100 K are in good accordance with the simulation, a strong deviation in the case of 2 is found. In both cases, the measured curves also show a bending to smaller  $\chi_{\text{M}}T$  values below 5 K, hinting towards an interaction, which is not covered by the simulation. An explanation for this is a residual of HS species at low temperatures, which is significantly higher in the case of 2. This will result in a way higher  $\chi_{\text{M}}T$  in the temperature range, where only the LS system is expected, than the  $\chi_{\text{M}}T$  value based on the EPR parameters.

In the case of 3, no SCO and a minor  $\chi_{\text{M}}T$  value was observed from 1.8 K up to 300 K. The LS state of  $\text{Fe}^{\text{II}}$  is  $S=0$  and hence not possessing any magnetic moment. Nevertheless with  $0.08 \text{ cm}^3\text{Kmol}^{-1}$ , a non-zero value of  $\chi_{\text{M}}T$  is found at 300 K. This is even lower than the theoretical value for an  $S=1/2$  system with  $g=2$  ( $0.375 \text{ cm}^3\text{Kmol}^{-1}$ ). As in the case of both  $\text{Co}^{\text{II}}$

compounds, this moment is attributed to a minor  $\text{Fe}^{\text{II}}$  HS amount of 2% in the sample (Figure S1).

## Conclusion

We successfully synthesized a new terpyridine ligand and a series of new terpyridine ligand based homoleptic  $\text{Co}^{\text{II}}$  and  $\text{Fe}^{\text{II}}$  complexes. The complexes were characterized and investigated through cyclic voltammetry, UV/Vis/NIR spectroelectrochemistry and EPR spectroscopy. The cyclic voltammogram revealed, that the substitution of the para-F by the backbone to the  $\text{NMe}_2$  group only has a marginal influence on the redox-potentials, but the different metal centers show redox processes at different potentials. Furthermore, the change of the solvent from  $\text{CH}_2\text{Cl}_2$  to  $\text{CH}_3\text{CN}$  leads to additional processes, which might be due to reaction with  $\text{CH}_3\text{CN}$  molecules during the measurement or an increased solvent window. The solid-state structure of complexes 1–3 was revealed by single crystal X-ray diffraction analysis. For complexes 1–3 the bond distances point towards a LS center at 100 K. Additionally, the SCO behavior was investigated through SQUID magnetometric measurements. Complexes 1 and 2 show a gradual SCO whereas complex 3 remains in the LS state over the measured temperature range. Furthermore, the  $^1\text{H}$  NMR spectra of complex 3 indicates that the  $\text{Fe}^{\text{II}}$  center is in its LS state at room temperature.

EPR measurement of complexes 1 and 2 show partially resolved hyperfine splittings that arise from interactions of the electron spin with the  $^{59}\text{Co}$  nucleus. This pattern was observed in the solid state and solution samples. The first reduction process of complexes 3 and 4 were investigated with EPR spectroelectrochemical measurements. The obtained signals show  $g$  values that are close to the one of the free electron, which supports the observation of a terpyridine-based process

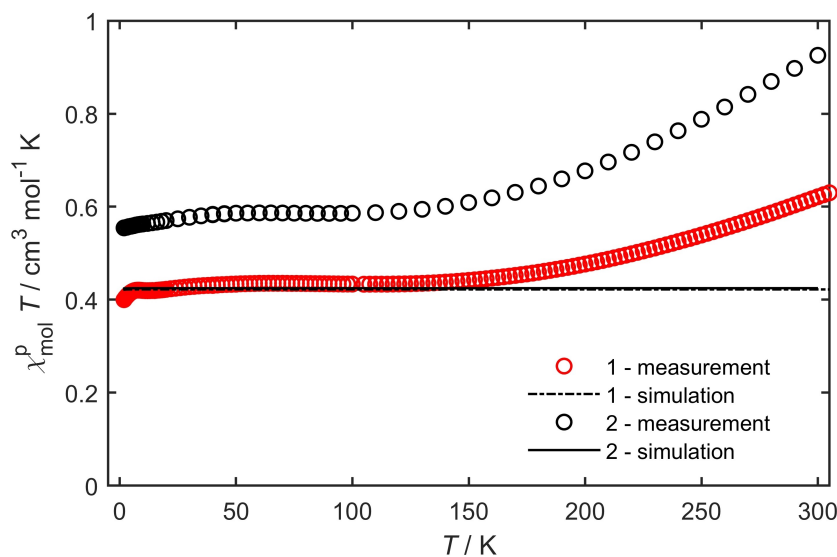


**Figure 8.** Temperature dependence of the  $\chi_{\text{M}}T$  product for 1 and 2 in an applied magnetic field of 1000 Oe as well as the corresponding LS spin Hamiltonian simulations.

for the iron complexes. In contrast, the first reduction process of the Co complexes is of a more mixed nature, which was confirmed by UV/Vis SEC measurements and quantum chemical calculations of complex **1**. Finally, all complexes were probed with polymerized optical microscopy regarding their liquid crystalline properties. Unfortunately, all complexes remained solid over the measured temperature range and thus no phase transitions could be observed.

## Experimental Section

**General Remarks and Instrumentation.** If noted, reactions were carried out using standard Schlenk-line techniques under an inert atmosphere of argon (Linde, HiQ Argon 5.0, purity  $\geq 99.999\%$ ). **Compounds:** Ligands **1** was synthesized following published procedures.<sup>[30]</sup> Commercially available chemicals were used without further purification. Dry DMF was available from Acros Organics (99.8% extra dry) and was used as received. Other dry solvents were available from MBRAUN MB-SPS- 800 solvent system and degassed by standard techniques prior to use. Column chromatography was conducted using aluminum oxide (Aluminum Oxide basic, Macherey-Nagel, 50–200  $\mu\text{m}$ ).  $^1\text{H}$  NMR, proton decoupled  $^{13}\text{C}$  and  $^{19}\text{F}$  NMR were recorded on JEOL ECS 400 spectrometer and JEOL ECZ 400R spectrometer. Chemical shifts are reported in ppm (relative to the TMS signal) with reference to the residual solvent peaks.<sup>[43]</sup> Multiplets are reported as follows: singlet (s), duplet (d), triplet (t), quartet (q), quintet (quint), septet (sept), and combinations thereof. Mass spectrometry was performed on an Agilent 6210 ESI-TOF. Elemental analysis was performed on a Perkin Elmer Analyser 240.

Cyclic voltammograms were recorded with a PAR VersaStat 4 potentiostat (Ametek) by working in anhydrous and degassed acetonitrile or dichloromethane with 0.1 M  $\text{NBu}_4\text{PF}_6$  (dried,  $>99.0\%$ , electrochemical grade, Fluka) as supporting electrolyte. Concentrations of the complexes were about  $1 \cdot 10^{-4}$  M. A three-electrode setup was used with a glassy carbon working electrode, a coiled platinum wire as counter electrode and a coiled silver wire as a pseudoreference electrode. The ferrocene/ferrocenium or decamethylferrocene/decamethylferrocenium couples were used as internal reference.

UV/Vis spectra were recorded with an Avantes spectrometer consisting of a light source (AvaLight-DH-S-Bal), a UV/VIS detector (AvaSpec-ULS2048), and an NIR detector (AvaSpec-NIR256-TEC) or on a J&M Tidas UV- Vis-NIR spectrophotometer. Spectroelectrochemical measurements were carried out in an optically transparent thin-layer electrochemical (OTTLE) cell ( $\text{CaF}_2$  windows) with a gold or platinum working electrode, a platinum mesh counter electrode, and a silver-foil pseudoreference electrode.<sup>[44]</sup> Anhydrous and degassed acetonitrile or dichloromethane with 0.1 M  $\text{NBu}_4\text{PF}_6$  as supporting electrolyte was used as solvent. An Autolab PGSTAT101 potentiostat (Metrohm) was used for all spectro-electrochemical measurements.

### Electron paramagnetic resonance

EPR spectra at X-band frequency (ca. 9.5 GHz) were obtained with a Magnettech MS-5000 benchtop EPR spectrometer equipped with a rectangular TE 102 cavity and TC HO4 temperature controller. The measurements were carried out in synthetic quartz glass tubes. For EPR spectro-electrochemistry a three-electrode setup was employed using two Teflon-coated platinum wires as working and counter electrodes and a Teflon-coated silver wire as pseudo-

reference electrode. Spectral simulations were performed with EasySpin 5.1.4<sup>7</sup> and MatLab R2012a.

### X-ray diffraction

X-ray data were collected on a Bruker Smart AXS or Bruker D8 Venture system at 100(2) K, respectively, using graphite-monochromated  $\text{Mo}\alpha$  radiation ( $\lambda = 0.71073 \text{ \AA}$ ). Using the Smart software or using the APEX2 software, respectively, evaluated the strategy for the data collection. The data were collected by the standard omega scan or omega + phi scan techniques, and were scaled and reduced using Saint + and SADABS software. Direct methods or intrinsic phasing using SHELXT-2014/7 solved the structures. Structures were refined by full matrix least-squares using OLEX2,<sup>[45]</sup> refining on F2. Non-hydrogen atoms were refined anisotropically.<sup>[46]</sup>

Deposition Numbers 2150337 (for **1**), 2150346 (for **2**), and 2150345 (for **3**) contain the supplementary crystallographic data for this paper. These data are provided free of charge by the joint Cambridge Crystallographic Data Centre and Fachinformationszentrum Karlsruhe Access Structures service.

### SQUID Magnetometry

All susceptibility measurements were carried out on a Quantum Design MPMS3 SQUID magnetometer. The measurements at a constant magnetic field of 1000 Oe in a temperature range from 1.8 K to 50 K and at 10 000 Oe in a temperature range from 40 K to 300 K. The measured data in the intersection of the temperature ranges served to compensate for possible ferromagnetic impurities. Samples were powdered with little pressure and mixed with eicosane. The mixture was melted in a capsule with a hot air gun maximized to a temperature of 50 °C (323.15 K) and the capsule was then fixed in a plastic tube. The temperature dependent measurements were limited to a temperature of 300 K due to the melting of the used eicosane matrix (melting point of eicosane: 311 K). Data were corrected for the diamagnetic contribution to the susceptibility by means of Pascal's constants.<sup>[47]</sup>

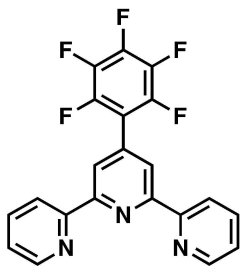
### Computational Details

All calculations have been performed using the TURBOMOLE program package, version 7.5.1 [TURBOMOLE V7.5 2020, a Development of University of Karlsruhe and Forschungszentrum Karlsruhe GmbH, 1989–2007, TURBOMOLE GmbH, since 2007; Available from <http://www.turbomole.com>].<sup>[48]</sup> Structures were optimized using the TPSS functional,<sup>[49]</sup> def2-TZVP basis sets,<sup>[50]</sup> including Grimme's D3 dispersion corrections<sup>[51]</sup> with Becke-Johnson damping<sup>[52]</sup> and the COSMO solvation model<sup>[53]</sup> with a dielectric constant of 8.94 for  $\text{CH}_2\text{Cl}_2$ . All calculations employed *gridsize* 3 and the multipole accelerated RIJ<sup>[54]</sup> approach in combination with the respective auxiliary basis sets.<sup>[53]</sup> Based on the excellent performance of the B97-D functional<sup>[56]</sup> in the recent benchmark study on SCO energies in Fe(II) complexes,<sup>[57]</sup> additional energy and TDDFT calculations were performed at the B97-D/def2-TZVP level.

For TDDFT spectra calculations, the ground-state SCF was converged until the energy changes were below  $10^{-8}$  Hartree, and the changes in the density matrix were below  $10^{-7}$ . A sufficient number of excitations were calculated so that the largest excitation energy covered was above 4.9 eV, which corresponds to  $\lambda = 250 \text{ nm}$ . The excitation energies were converged until the remaining residue was below  $10^{-4}$ .

## Synthesis

### TPY-PhF<sub>5</sub> L1



The synthesis was performed according to a literature known procedure.<sup>[1]</sup>

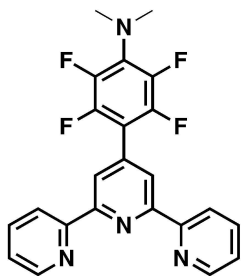
2,3,4,5,6-pentafluorobenzaldehyde (586.3 mg, 3.0 mmol) was dissolved in ethanol (20 mL), 2-acetylpyridine (848.0 mg, 0.7 mmol) and KOH (390.0 mg, 7.0 mmol) were added. 25 mL of concentrated ammonia solution was added and the mixture was stirred at room temperature over night. The resulting solid was filtered and washed with cold water and ethanol yielding in the desired product as yellow solid (199.8 mg, 0.5 mmol, 71 %).

The <sup>1</sup>H NMR spectrum is similar to the spectrum literature (recorded in CDCl<sub>3</sub>).<sup>[58]</sup>

<sup>1</sup>H NMR (DMSO, 400 MHz, 21 °C): δ = 8.73 (dq, <sup>3</sup>J = 9.2, 1.1 Hz, 2 H), 8.70–8.65 (m, 4 H), 7.93 (td, J = 7.7, 1.8 Hz, 2 H), 7.44–7.34 (m, 2 H) ppm.

<sup>19</sup>F (DMSO, 400 MHz, 21 °C): δ = –142.80, –145.82, –156.45, –157.99, –164.16 ppm.

### TPY-PhF<sub>4</sub>NMe<sub>2</sub> L2



4'-(perfluorophenyl)-2,2':6',2''-terpyridine (199.6 mg, 0.5 mmol) and K<sub>2</sub>CO<sub>3</sub> (276.4 g, 2.0 mmol) were dissolved in dry *N,N*-dimethylformamide (10 mL). The mixture was stirred at 90 °C for one week. After cooling to room temperature CH<sub>2</sub>Cl<sub>2</sub> (30 mL) was added and extracted with water and brine (30 mL). The crude product was purified by column chromatography (basic Al<sub>2</sub>O<sub>3</sub>, CH<sub>2</sub>Cl<sub>2</sub>). The solvent was evaporated, the resulting solid dissolved in CH<sub>2</sub>Cl<sub>2</sub> and precipitated in *n*-pentane. After filtration the solvent was evaporated yielding in a yellow solid (86.0 mg, 0.2 mmol, 41 %).

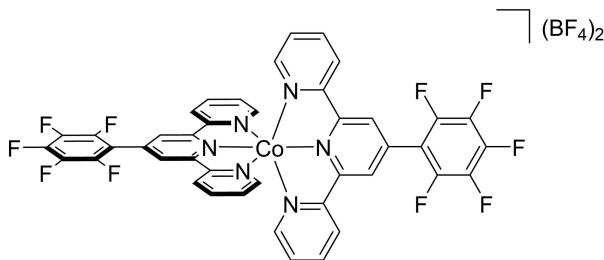
<sup>1</sup>H NMR (CDCl<sub>3</sub>, 400 MHz, 24 °C): δ = 8.70 (d, <sup>3</sup>J = 4.8 Hz, 2 H), 8.66 (dd, <sup>3</sup>J = 8.0, 4.3 Hz, 2 H), 8.57 (s, 2 H), 7.93–7.84 (m, 2 H), 7.41–7.29 (m, 2 H), 4.43–4.35 (m, 3 H), 1.47 (t, <sup>3</sup>J = 7.0 Hz, 3 H) ppm.

<sup>19</sup>F NMR (CDCl<sub>3</sub>, 376 MHz, 23 °C): δ = –141.99 (dd, J = 22.7, 7.7 Hz), –143.26–(–144.01) (m), –144.45 – (145.17) (m), –151.51 (d, J = 12.3 Hz), –153.02 (t, J = 21.3 Hz), –156.68 – (–156.86) (m), –161.17 (dd, J = 21.2, 7.6 Hz) ppm.

<sup>13</sup>C NMR (CDCl<sub>3</sub>, 101 MHz, 27 °C) δ = 15.5, 43.3, 71.1, 121.4, 122.2, 124.1, 124.1, 137.0, 149.4, 155.8, 156.1 ppm.

HRMS (ESI): calcd. For [C<sub>23</sub>H<sub>17</sub>F<sub>4</sub>N<sub>4</sub>]<sup>+</sup> [M–H]<sup>+</sup>: 425.1384 *m/z*; found 425.1385.

### [Co(TpyPhF<sub>5</sub>)(BF<sub>4</sub>)<sub>2</sub>] 1

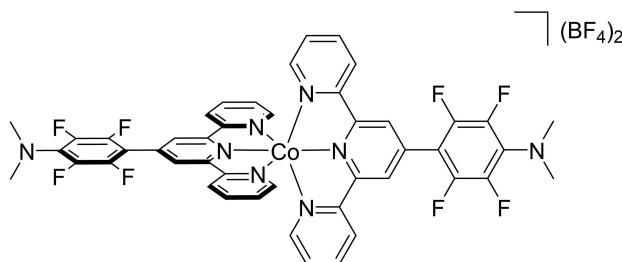


Co(BF<sub>4</sub>)<sub>2</sub>·6 H<sub>2</sub>O (170.3 mg, 0.5 mmol) was dissolved in 30 mL MeOH and 4'-(perfluorophenyl)-2,2':6',2''-terpyridine (399.0 mg, 1.0 mmol) was added. The mixture was stirred for two days, the solvent was evaporated and the crude product was dissolved in acetonitrile and precipitated in ethanol, yielding in a red solid (399.0 mg, 0.4 mmol, 76 %). Crystals suitable for X-ray diffraction were grown by slow diffusion of diethylether in an acetonitrile solution of the complex.

HRMS (ESI): calcd. For [C<sub>42</sub>H<sub>20</sub>CoF<sub>10</sub>N<sub>6</sub>]<sup>2+</sup>: *m/z* 428.5455; found 428.5488.

Anal. Calcd for C<sub>42</sub>H<sub>20</sub>B<sub>2</sub>CoF<sub>18</sub>N<sub>6</sub>: C, 48.92; H, 1.96; N, 8.15. Found: C, 48.94; H, 2.00; N, 8.17.

### [Co(TpyPhF<sub>4</sub>NMe<sub>2</sub>)<sub>2</sub>](BF<sub>4</sub>)<sub>2</sub> 2

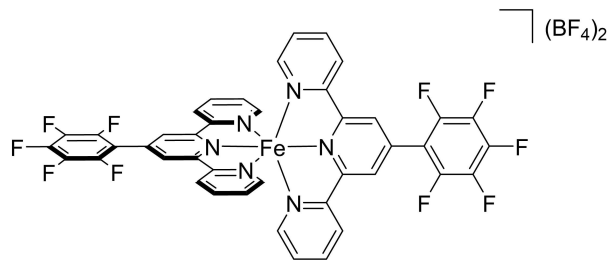


Co(BF<sub>4</sub>)<sub>2</sub>·6 H<sub>2</sub>O (49.40 mg, 0.15 mmol) was dissolved in 5 mL MeOH and 4-([2,2':6',2''-terpyridin]-4'-yl)-2,3,5,6-tetrafluoro-*N,N*-dimethylaniline (121.3 mg, 0.29 mmol) was added. The mixture was stirred for one week, the solvent was evaporated and the crude product was dissolved in acetonitrile and precipitated in diethylether, yielding in a red solid (100.10 mg, 0.09 mmol, 62 %). Crystals suitable for X-ray diffraction were grown by slow diffusion of diethylether in an acetonitrile solution of the complex.

HRMS (ESI): calcd. For [C<sub>46</sub>H<sub>32</sub>CoF<sub>8</sub>N<sub>8</sub>]<sup>2+</sup>: *m/z* 453.5972; found 453.6017.

Anal. Calcd for C<sub>46</sub>H<sub>32</sub>B<sub>2</sub>F<sub>16</sub>CoN<sub>8</sub>: C, 51.09; H, 2.98; N, 10.36. Found: C, 51.23; H, 3.25; N, 10.66.

**[Fe(TpyPhF<sub>2</sub>)<sub>2</sub>](BF<sub>4</sub>)<sub>2</sub> 3**



Fe(BF<sub>4</sub>)<sub>2</sub>·6 H<sub>2</sub>O (168.7 mg, 0.5 mmol) was dissolved in 10 mL MeOH and 4'-((perfluorophenyl)-2,2':6',2''-terpyridine (399.0 mg, 1.0 mmol) was added. The mixture was stirred for four days, the solvent was evaporated and the crude product was dissolved in acetonitrile and precipitated in ethanol, yielding in a purple solid (439.5 mg, 0.4 mmol, 85%). Crystals suitable for X-ray diffraction were grown by slow diffusion of diethylether in an acetonitrile solution of the complex.

<sup>1</sup>H NMR (CD<sub>3</sub>CN, 400 MHz, 21 °C): δ = 9.06 (s, 4 H), 8.50 (s, 4 H), 7.92 (s, 4 H), 7.15 (d, <sup>3</sup>J = 20.7 Hz, 8 H) ppm.

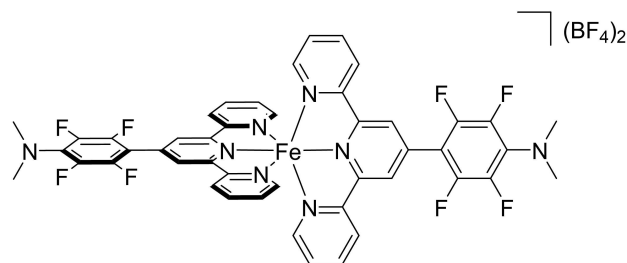
<sup>19</sup>F NMR (CD<sub>3</sub>CN, 377 MHz, 19 °C): δ = -142.6, -144.8, -151.7, -152.8, -157.9, -162.8 ppm.

<sup>13</sup>C NMR (CD<sub>3</sub>CN, 151 MHz, 25 °C): δ = 161.5, 161.3, 158.3, 158.2, 154.2, 139.9, 128.6, 128.5, 125.3, 125.1, 72.4, 15.7 ppm.

HRMS (ESI): calcd. For [C<sub>42</sub>H<sub>20</sub>CoF<sub>10</sub>N<sub>6</sub>]<sup>2+</sup>: m/z 427.0464; found 427.0491.

Anal. Calcd for C<sub>42</sub>H<sub>20</sub>B<sub>2</sub>F<sub>18</sub>FeN<sub>6</sub>·1.65 H<sub>2</sub>O·0.15 C<sub>2</sub>H<sub>3</sub>N: C, 47.75; H, 2.25; N, 8.10. Found: C, 47.61; H, 2.09; N, 8.24.

**[Fe(TpyPhF<sub>4</sub>NMe<sub>2</sub>)<sub>2</sub>](BF<sub>4</sub>)<sub>2</sub> 4**



Fe(BF<sub>4</sub>)<sub>2</sub>·6 H<sub>2</sub>O (47.8 mg, 0.14 mmol) was dissolved in 5 mL MeOH and 4-((2,2':6',2''-terpyridin-4'-yl)-2,3,5,6-tetrafluoro-N,N-dimethylaniline (120.4 mg, 0.28 mmol) was added. The mixture was stirred for one week, the solvent was evaporated and the crude product was dissolved in acetonitrile and precipitated in diethylether, yielding in a purple solid (74.80 mg, 0.07 mmol, 50%).

<sup>1</sup>H NMR (CD<sub>3</sub>CN, 401 MHz, 19 °C): δ = 9.06 (s, 4 H), 8.46 (t, <sup>3</sup>J = 8.3 Hz, 4 H), 7.87 (m, 4 H), 7.14 (d, <sup>3</sup>J = 5.6 Hz, 4 H), 7.08 (d, <sup>3</sup>J = 5.9 Hz, 8 H), 4.53 (q, <sup>3</sup>J = 7.0 Hz, 4 H), 1.48 (t, <sup>3</sup>J = 7.0 Hz, 4 H) ppm.

<sup>19</sup>F NMR (CD<sub>3</sub>CN, 377 MHz, 19 °C): δ = -144.73, -151.17, -157.36 ppm.

<sup>13</sup>C NMR (CD<sub>3</sub>CN, 151 MHz, 25 °C): δ = 161.5, 158.4, 154.3, 140.0, 128.6, 128.3, 125.3, 125.1, 111.0, 72.5, 15.8 ppm.

Anal. Calcd for C<sub>46</sub>H<sub>32</sub>B<sub>2</sub>F<sub>16</sub>FeN<sub>8</sub>·0.55 C<sub>4</sub>H<sub>10</sub>O·0.3 CH<sub>2</sub>Cl<sub>2</sub>: C, 50.90; H, 3.36; N, 9.79. Found: C, 51.28; H, 2.97; N, 9.39.

**Supporting Information**

Additional references cited within the Supporting Information.<sup>[59–64]</sup>

**Acknowledgements**

We would like to thank Prof. Dr. Sabine Laschat and Eugen Wuckert for the POM measurements of the complexes. We would like to thank Fridolin Hennhöfer for the help with the EPR SEC measurements. We would like to acknowledge the assistance of the Core Facility BioSupraMol supported by the DFG. Funded by the Deutsche Forschungsgemeinschaft [DFG, German Research Foundation – Project-ID 387284271 – SFB 1349]. Open Access funding enabled and organized by Projekt DEAL.

**Conflict of Interest**

The authors declare no conflict of interest.

**Data Availability Statement**

The data that support the findings of this study are available in the supplementary material of this article.

**Keywords:** cobalt · electrochemistry · fluorinated terpyridine · iron · spin crossover

[1] a) U. S. Schubert, H. Hofmeier, G. R. Newkome, *Modern Terpyridine Chemistry*, Wiley-VCH, Weinheim, **2006**; b) H. Hofmeier, U. S. Schubert, *Chem. Soc. Rev.* **2004**, *33*, 373–399.  
 [2] G. T. Morgan, F. H. Burstall, *J. Chem. Soc.* **1932**, 20–30.  
 [3] a) P. E. Rosevear, W. H. F. Sasse, *J. Heterocycl. Chem.* **1971**, *8*, 483–485; b) M. T. Robo, M. R. Prinsell, D. J. Weix, *J. Org. Chem.* **2014**, *79*, 10624–10628.  
 [4] a) T. Hiyama, *Metal-Catalyzed Cross-Coupling Reactions* Wiley-VCH, Weinheim, Germany, **1998**; b) T. Hiyama, Y. Hatanaka, *Pure Appl. Chem.* **1994**, *66*, 1471–1478; c) T. Hiyama, *J. Organomet. Chem.* **2002**, *653*, 58–61.  
 [5] a) R.-A. Fallahpour, *Synthesis* **2000**, 1665–1667; b) R. García-Lago, J. Alonso-Gómez, C. C. Sicre, M.-M. Cid, *Heterocycles* **2008**, *75*, 57–64; c) M. Benaglia, S. Toyota, C. R. Woods, J. S. Siegel, *Tetrahedron Lett.* **1997**, *38*, 4737–4740.  
 [6] I. Sasaki, J. C. Daran, G. G. A. Balavoine, *Synthesis* **1999**, 1999, 815–820.  
 [7] a) S. Aroua, T. K. Todorova, P. Hommes, L.-M. Chamoreau, H.-U. Reissig, V. Mougél, M. Fontecave, *Inorg. Chem.* **2017**, *56*, 5930–5940; b) P. Hommes, C. Fischer, C. Lindner, H. Zipse, H.-U. Reissig, *Angew. Chem. Int. Ed.* **2014**, *53*, 7647–7651; *Angew. Chem.* **2014**, *126*, 7778–7782; c) J. R. Colombe, S. Bernhardt, C. Stathakis, S. L. Buchwald, P. Knochel, *Org. Lett.* **2013**, *15*, 5754–5757.  
 [8] a) N. Elgrishi, S. Griveau, M. B. Chambers, F. Bedioui, M. Fontecave, *Chem. Commun.* **2015**, *51*, 2995–2998; b) N. Elgrishi, M. B. Chambers, M. Fontecave, *Chem. Sci.* **2015**, *6*, 2522–2531.  
 [9] N. Elgrishi, M. B. Chambers, V. Artero, M. Fontecave, *Phys. Chem. Chem. Phys.* **2014**, *16*, 13635–13644.  
 [10] R. Tatikonda, M. Cametti, E. Kalenius, A. Famulari, K. Rissanen, M. Haukka, *Eur. J. Inorg. Chem.* **2019**, *2019*, 4463–4470.  
 [11] a) S. G. Shepard, S. M. Fatur, A. K. Rappé, N. H. Damrauer, *J. Am. Chem. Soc.* **2016**, *138*, 2949–2952; b) D. G. Brown, N. Sanguantrakun, B. Schulze, U. S. Schubert, C. P. Berlinguette, *J. Am. Chem. Soc.* **2012**, *134*,

- 12354–12357; c) H.-W. Lin, Y.-S. Wang, Z.-Y. Huang, Y.-M. Lin, C.-W. Chen, S.-H. Yang, K.-L. Wu, Y. Chi, S.-H. Liu, P.-T. Chou, *Phys. Chem. Chem. Phys.* **2012**, *14*, 14190–14195.
- [12] a) J.-H. Yum, E. Baranoff, F. Kessler, T. Moehl, S. Ahmad, T. Bessho, A. Marchiori, E. Ghadiri, J.-E. Moser, C. Yi, M. K. Nazeeruddin, M. Grätzel, *Nat. Commun.* **2012**, *3*, 631; b) S. A. Sapp, C. M. Elliott, C. Contado, S. Caramori, C. A. Bignozzi, *J. Am. Chem. Soc.* **2002**, *124*, 11215–11222.
- [13] a) Z. Zheng, L. Opilik, F. Schiffrmann, W. Liu, G. Bergamini, P. Ceroni, L.-T. Lee, A. Schütz, J. Sakamoto, R. Zenobi, J. VandeVondele, A. D. Schlüter, *J. Am. Chem. Soc.* **2014**, *136*, 6103–6110; b) G. Gröger, W. Meyer-Zaika, C. Böttcher, F. Gröhn, C. Ruthard, C. Schmuck, *J. Am. Chem. Soc.* **2011**, *133*, 8961–8971; c) U. S. Schubert, C. Eschbaumer, *Angew. Chem. Int. Ed.* **2002**, *41*, 2892–2926; *Angew. Chem.* **2002**, *114*, 3016–3050; d) F. Chen, Y.-K. Tian, Y. Chen, *Chem. Asian J.* **2018**, *13*, 3169–3172.
- [14] J. Tan, R. Li, D. Li, Q. Zhang, S. Li, H. Zhou, J. Yang, J. Wu, Y. Tian, *Dalton Trans.* **2015**, *44*, 1473–1482.
- [15] A. Fermi, G. Bergamini, M. Roy, M. Gingras, P. Ceroni, *J. Am. Chem. Soc.* **2014**, *136*, 6395–6400.
- [16] C. S. Sevov, S. L. Fisher, L. T. Thompson, M. S. Sanford, *J. Am. Chem. Soc.* **2016**, *138*, 15378–15384.
- [17] a) S. J. Lippard, *Acc. Chem. Res.* **1978**, *11*, 211–217; b) P. M. van Vliet, S. M. S. Toekimin, J. G. Haasnoot, J. Reedijk, O. Nováková, O. Vrána, V. Brabec, *Inorg. Chim. Acta* **1995**, *231*, 57–64; c) I. Eryazici, C. N. Moorefield, G. R. Newkome, *Chem. Rev.* **2008**, *108*, 1834–1895.
- [18] K. Senthil Kumar, M. Ruben, *Coord. Chem. Rev.* **2017**, *346*, 176–205.
- [19] a) O. Sato, *Nat. Chem.* **2016**, *8*, 644–656; b) M. A. Halcrow, *Spin-crossover materials. Properties and application*, Wiley, Chichester, **2013**; c) P. Gütllich, H. A. Goodwin, *Spin Crossover in Transition Metal Compounds I, II, and III*, Springer, Berlin, Germany, **2004**.
- [20] D. Shao, L. Shi, F.-X. Shen, X.-Q. Wei, O. Sato, X.-Y. Wang, *Inorg. Chem.* **2019**, *58*, 11589–11598.
- [21] a) P. Silva, S. M. F. Vilela, J. P. C. Tomé, F. A. Almeida Paz, *Chem. Soc. Rev.* **2015**, *44*, 6774–6803; b) C.-L. Ho, Z.-Q. Yu, W.-Y. Wong, *Chem. Soc. Rev.* **2016**, *45*, 5264–5295; c) M. Castellano, R. Ruiz-García, J. Cano, J. Ferrando-Soria, E. Pardo, F. R. Fortea-Pérez, S.-E. Stiriba, W. P. Barros, H. O. Stumpf, L. Cañadillas-Delgado, J. Pasán, C. Ruiz-Pérez, G. de Munno, D. Armentano, Y. Journaux, F. Lloret, M. Julve, *Coord. Chem. Rev.* **2015**, *303*, 110–138; d) M. K. Singh, Y. Yang, C. G. Takoudis, *Coord. Chem. Rev.* **2009**, *253*, 2920–2934; e) E. Chelebaeva, J. Larionova, Y. Guari, R. A. S. Ferreira, L. D. Carlos, F. A. A. Paz, A. Trifonov, C. Guérin, *Inorg. Chem.* **2009**, *48*, 5983–5995; f) J. Long, J. Rouquette, J. M. Thibaud, R. A. Ferreira, L. D. Carlos, F. Donnadieu, V. Vieru, L. F. Chibotaru, L. Konczewicz, J. Haines, Y. Guari, J. Larionova, *Angew. Chem. Int. Ed.* **2015**, *54*, 2236–2240; *Angew. Chem.* **2015**, *127*, 2264–2268.
- [22] a) C. Faulmann, K. Jacob, S. Dorbes, S. Lampert, I. Malfant, M.-L. Doublet, L. Valade, J. A. Real, *Inorg. Chem.* **2007**, *46*, 8548–8559; b) K. Takahashi, H.-B. Cui, Y. Okano, H. Kobayashi, H. Mori, H. Tajima, Y. Einaga, O. Sato, *J. Am. Chem. Soc.* **2008**, *130*, 6688–6689; c) M. Nihei, N. Takahashi, H. Nishikawa, H. Oshio, *Dalton Trans.* **2011**, *40*, 2154–2156; d) S. M. B. H. Phan, E. Steven, J. S. Brooks, M. Shatruck, *Angew. Chem. Int. Ed.* **2015**, *54*, 823–827; *Angew. Chem.* **2015**, *127*, 837–841.
- [23] a) S. Hayami, R. Moriyama, A. Shuto, Y. Maeda, K. Ohta, K. Inoue, *Inorg. Chem.* **2007**, *46*, 7692–7694; b) M. Seredyuk, A. B. Gaspar, V. Ksenofontov, Y. Galyametdinov, J. Kusz, P. Gütllich, *Adv. Funct. Mater.* **2008**, *18*, 1089–2101; c) M. Seredyuk, A. B. Gaspar, V. Ksenofontov, Y. Galyametdinov, J. Kusz, P. Gütllich, *J. Am. Chem. Soc.* **2008**, *130*, 1431–1439; d) A. B. Gaspar, M. Seredyuk, P. Gütllich, *Coord. Chem. Rev.* **2009**, *253*, 2399–2413; e) R. Akiyoshi, Y. Hirota, D. Kosumi, M. Tsutsumi, M. Nakamura, L. F. Lindoy, S. Hayami, *Chem. Sci.* **2019**, *10*, 5843–5848.
- [24] a) A. B. Gaspar, V. Ksenofontov, M. Seredyuk, P. Gütllich, *Coord. Chem. Rev.* **2005**, *249*, 2661–2676; b) S. Bonhommeau, P. G. Lacroix, D. Talaga, A. Bousseksou, M. Seredyuk, I. O. Fritsky, Y. Rodriguez, *J. Phys. Chem. C* **2012**, *116*, 11251–11255; c) W. Liu, X. Bao, L.-L. Mao, J. Tucek, R. Zboril, J.-L. Liu, F.-S. Guo, Z.-P. Ni, M.-L. Tong, *Chem. Commun.* **2014**, *50*, 4059–4061.
- [25] a) I. Suleimanov, O. Kraieva, J. Sánchez Costa, I. O. Fritsky, G. Molnár, L. Salmon, A. Bousseksou, *J. Mater. Chem. C* **2015**, *3*, 5026–5032; b) A. Santoro, L. J. Kershaw Cook, R. Kulmaczewski, S. A. Barrett, O. Cespedes, M. A. Halcrow, *Inorg. Chem.* **2015**, *54*, 682–693; c) C. F. Wang, R. F. Li, X. Y. Chen, R. J. Wei, L. S. Zheng, J. Tao, *Angew. Chem. Int. Ed.* **2015**, *54*, 1574–1577; d) M. Estrader, J. S. Uber, L. A. Barrios, J. Garcia, P. Lloyd-Williams, O. Roubeau, S. J. Teat, G. Aromi, *Angew. Chem. Int. Ed.* **2017**, *56*, 15622–15627; *Angew. Chem.* **2017**, *129*, 15828–15833; e) J.-Y. Ge, Z. Chen, L. Zhang, X. Liang, J. Su, M. Kurmoo, J.-L. Zuo, *Angew. Chem. Int. Ed.* **2019**, *58*, 8789–8793; f) B. Benaicha, K. Van Do, A. Yangui, N. Pittala, A. Lusson, M. Sy, G. Bouchez, H. Fourati, C. J. Gómez-García, S. Triki, K. Boukhehdaden, *Chem. Sci.* **2019**, *10*, 6791–6798.
- [26] R. Akiyoshi, Y. Komatsumaru, M. Donoshita, S. Dekura, Y. Yoshida, H. Kitagawa, Y. Kitagawa, L. F. Lindoy, S. Hayami, *Angew. Chem. Int. Ed.* **2021**, *60*, 12717–12722; *Angew. Chem.* **2021**, *133*, 12827–12832.
- [27] S. Hayami, Y. Shigeyoshi, M. Akita, K. Inoue, K. Kato, K. Osaka, M. Takata, R. Kawajiri, T. Mitani, Y. Maeda, *Angew. Chem. Int. Ed.* **2005**, *44*, 4899–4903; *Angew. Chem.* **2005**, *117*, 4977–4981.
- [28] J. A. Kitchen, N. G. White, C. Gandolfi, M. Albrecht, G. N. L. Jameson, J. L. Tallon, S. Brooker, *Chem. Commun.* **2010**, *46*, 6464–6466.
- [29] a) S. Hayami, K. Kato, Y. Komatsu, A. Fuyuhito, M. Ohba, *Dalton Trans.* **2011**, *40*, 2167–2169; b) S. Hayami, D. Urakami, Y. Kojima, H. Yoshizaki, Y. Yamamoto, K. Kato, A. Fuyuhito, S. Kawata, K. Inoue, *Inorg. Chem.* **2010**, *49*, 1428–1432; c) Y. Komatsu, K. Kato, Y. Yamamoto, H. Kamihata, Y. H. Lee, A. Fuyuhito, S. Kawata, S. Hayami, *Eur. J. Inorg. Chem.* **2012**, *2012*, 2769–2775; d) S. Hayami, Y. Komatsu, T. Shimizu, H. Kamihata, Y. H. Lee, *Coord. Chem. Rev.* **2011**, *255*, 1981–1990; e) S. Hayami, R. Moriyama, Y. Shigeyoshi, R. Kawajiri, T. Mitani, M. Akita, K. Inoue, Y. Maeda, *Inorg. Chem.* **2005**, *44*, 7295–7297; f) S. Hayami, K. Murata, D. Urakami, Y. Kojima, M. Akita, K. Inoue, *Chem. Commun.* **2008**, 6510–6512.
- [30] O. A. Oyetade, V. O. Nyamori, B. S. Martincigh, S. B. Jonnalagadda, *RSC Adv.* **2016**, *6*, 2731–2745.
- [31] a) E. C. Constable, in *Adv. Inorg. Chem. Radiochem., Vol. 30* (Ed.: H. J. Emeléus), Academic Press, **1986**, pp. 69–121; b) A. T. Baker, H. A. Goodwin, *Aust. J. Chem.* **1985**, *38*, 207–214; c) P. Laine, A. Gourdoin, J. P. Launay, *Inorg. Chem.* **1995**, *34*, 5156–5165; d) Y. Nakayama, Y. Baba, H. Yasuda, K. Kawakita, N. Ueyama, *Macromolecules* **2003**, *36*, 7953–7958; e) S. K. Hain, F. W. Heinemann, K. Gieb, P. Müller, G. Hörner, A. Grohmann, *Eur. J. Inorg. Chem.* **2010**, *2010*, 221–232; f) L. J. Kershaw Cook, F. Tuna, M. A. Halcrow, *Dalton Trans.* **2013**, *42*, 2254–2265.
- [32] R. J. Davidson, E. W. Ainscough, A. M. Brodie, G. B. Jameson, M. R. Waterland, H. R. Allcock, M. D. Hindenlang, B. Moubaraki, K. S. Murray, K. C. Gordon, R. Horvath, G. N. L. Jameson, *Inorg. Chem.* **2012**, *51*, 8307–8316.
- [33] I. F. Mansoor, D. I. Wozniak, Y. Wu, M. C. Lipke, *Chem. Commun.* **2020**, 56, 13864–13867.
- [34] J. Chambers, B. Eaves, D. Parker, R. Claxton, P. S. Ray, S. J. Slattery, *Inorg. Chim. Acta* **2006**, *359*, 2400–2406.
- [35] H. Ferreira, M. M. Conradie, J. Conradie, *Inorg. Chim. Acta* **2019**, *486*, 26–35.
- [36] B. de Bruin, E. Bill, E. Bothe, T. Weyhermüller, K. Wieghardt, *Inorg. Chem.* **2000**, *39*, 2936–2947.
- [37] J. Klein, A. Stuckmann, S. Sobottka, L. Suntrup, M. van der Meer, P. Hommes, H.-U. Reissig, B. Sarkar, *Chem. Eur. J.* **2017**, *23*, 12314–12325.
- [38] J. England, E. Bill, T. Weyhermüller, F. Neese, M. Atanasov, K. Wieghardt, *Inorg. Chem.* **2015**, *54*, 12002–12018.
- [39] S. Kremer, W. Henke, D. Reinen, *Inorg. Chem.* **1982**, *21*, 3013–3022.
- [40] P. Nielsen, H. Toftlund, A. D. Bond, J. F. Boas, J. R. Pilbrow, G. R. Hanson, C. Noble, M. J. Riley, S. M. Neville, B. Moubaraki, K. S. Murray, *Inorg. Chem.* **2009**, *48*, 7033–7047.
- [41] B. Odom, D. Hanneke, B. D'Urso, G. Gabrielse, *Phys. Rev. Lett.* **2006**, *97*, 030801.
- [42] a) J. A. Real, A. B. Gaspar, M. C. Muñoz, *Dalton Trans.* **2005**, 2062–2079; b) O. Sato, J. Tao, Y.-Z. Zhang, *Angew. Chem. Int. Ed.* **2007**, *46*, 2152–2187; *Angew. Chem.* **2007**, *119*, 2200–2236; c) M. A. Halcrow, *Chem. Soc. Rev.* **2011**, *40*, 4119–4142.
- [43] G. R. Fulmer, A. J. M. Miller, N. H. Sherden, H. E. Gottlieb, A. Nudelman, B. M. Stoltz, J. E. Bercaw, K. I. Goldberg, *Organometallics* **2010**, *29*, 2176–2179.
- [44] M. Krejčík, M. Daněk, F. Hartl, *J. Electroanal. Chem.* **1991**, *317*, 179–187.
- [45] L. J. B. O. V. Dolomanov, R. J. Gildea, J. A. K. Howard, H. Puschmann, *J. Appl. Crystallogr.* **2009**, *42*, 339–341.
- [46] a) G. M. Sheldrick, *SHELXS-97, Program for Crystal Structure Solution and Refinement*, 1997, University of Göttingen, Germany; b) G. Sheldrick, *Acta Crystallogr. Sect. A* **2008**, *64*, 112–122; c) G. M. Sheldrick, *SADABS Ver. 2008/1, SADABS. Program for Empirical Absorption Correction* 2012, University of Göttingen, Germany; d) G. M. Sheldrick, *SHELXL Version 2014/7, Program for Crystal Structure Solution and Refinement* 2014, University of Göttingen, Germany; e) G. Sheldrick, *Acta Crystallogr. Sect. C* **2015**, *71*, 3–8; f) A. Spek, *J. Appl. Crystallogr.* **2003**, *36*, 7–13; g) SAINT+, *Data Integration Engine, Version 8.27b*, Bruker AXS, Madison, Wisconsin, USA, 1997–2012; h) S. W. Kwok, J. R. Fotsing, R. J. Fraser, V. O. Rodionov, V. V. Fokin, *Org. Lett.* **2010**, *12*, 4217–4219.
- [47] G. A. Bain, J. F. Berry, *J. Chem. Educ.* **2008**, *85*, 532.

- [48] S. G. Balasubramani, G. P. Chen, S. Coriani, M. Diedenhofen, M. S. Frank, Y. J. Franzke, F. Furche, R. Grotjahn, M. E. Harding, C. Hättig, A. Hellweg, B. Helmich-Paris, C. Holzer, U. Huniar, M. Kaupp, A. M. Khah, S. K. Khani, T. Müller, F. Mack, B. D. Nguyen, S. M. Parker, E. Perlt, D. Rappoport, K. Reiter, S. Roy, M. Rückert, G. Schmitz, M. Sierka, E. Tapavicza, D. P. Tew, C. v. Wüllen, V. K. Voora, F. Weigend, A. Wodyński, J. M. Yu, *J. Chem. Phys.* **2020**, *152*, 184107.
- [49] J. Tao, J. P. Perdew, V. N. Staroverov, G. E. Scuseria, *Phys. Rev. Lett.* **2003**, *91*, 146401.
- [50] F. Weigend, R. Ahlrichs, *Phys. Chem. Chem. Phys.* **2005**, *7*, 3297–3305.
- [51] S. Grimme, J. Antony, S. Ehrlich, H. Krieg, *J. Chem. Phys.* **2010**, *132*, 154104.
- [52] S. Grimme, S. Ehrlich, L. Goerigk, *J. Comput. Chem.* **2011**, *32*, 1456–1465.
- [53] A. Klamt, G. Schüürmann, *J. Chem. Soc. Perkin Trans. 2* **1993**, 799–805.
- [54] M. Sierka, A. Hogekamp, R. Ahlrichs, *J. Chem. Phys.* **2003**, *118*, 9136–9148.
- [55] F. Weigend, *Phys. Chem. Chem. Phys.* **2006**, *8*, 1057–1065.
- [56] S. Grimme, *J. Chem. Phys.* **2006**, *124*, 034108.
- [57] M. Reimann, M. Kaupp, *J. Chem. Theory Comput.* **2022**, *18*, 7442–7456.
- [58] E. C. Constable, B. Kariuki, A. Mahmood, *Polyhedron* **2003**, *22*, 687–698.
- [59] C. Adamo, V. Barone, *J. Chem. Phys.* **1999**, *110*, 6158–6170.
- [60] J.-D. Chai, M. Head-Gordon, *Phys. Chem. Chem. Phys.* **2008**, *10*, 6615–6620.
- [61] M. Haasler, T. M. Maier, R. Grotjahn, S. Gückel, A. V. Arbuznikov, M. Kaupp, *J. Chem. Theory Comput.* **2020**, *16*, 5645–5657.
- [62] S. Grimme, *J. Chem. Phys.* **2006**, *124*, 034108.
- [63] M. Reimann, M. Kaupp, *J. Chem. Theory Comput.* **2022**, *18*, 7442–7456.
- [64] a) S. Aroua, T. K. Todorova, P. Hommes, L.-M. Chamoreau, H.-U. Reissig, V. Mougél, M. Fontecave, *Inorg. Chem.* **2017**, *56*, 5930–5940; b) S. Aroua, T. K. Todorova, V. Mougél, P. Hommes, H.-U. Reissig, M. Fontecave, *ChemCatChem* **2017**, *9*, 2099–2105.

---

Manuscript received: February 21, 2023  
Revised manuscript received: April 1, 2023  
Accepted manuscript online: April 4, 2023